



## Research article

# A novel growth-friendly system alleviates pulmonary dysplasia in early-onset scoliosis combined with thoracic insufficiency syndrome: Radiological, pathological, and transcriptomic assessments

Ying Zhang, Quan Li, Zhiyue Shi, Qitang Li, Xinfei Dai, Cheng Pan, Yujian Ma, Rongshuang Yan, Derui Fei, Jingming Xie<sup>\*</sup>

Department of Orthopaedics, the Second Affiliated Hospital of Kunming Medical University, China

## ARTICLE INFO

**Keywords:**

Early-onset scoliosis  
Thoracic insufficiency syndrome  
Growing rod  
Pulmonary hypoplasia  
Radiology  
Pathology  
Transcriptomics

## ABSTRACT

**Background:** The posterior procedure utilizing growth-friendly techniques is the golden standard for patients with early-onset scoliosis combined with thoracic insufficiency syndrome (EOS + TIS). Pulmonary hypoplasia is the main cause of dying prematurely in the EOS + TIS. This study assessed the therapeutic impact of a novel growth-friendly system on the pulmonary development of piglet's EOS + TIS model.

**Methods:** The animal procedure period lasts 12 weeks, of which the construction of the EOS + TIS was performed at 0–8 weeks, and implantation of a novel growth-friendly system was applied at 8–12 weeks. During the animal procedure, X-rays and CT were performed to observe scoliosis, thorax, and lungs. After 12 weeks, pathological changes in lung tissue were assessed using HE and IHC staining. RNA-seq characterized novel growth-friendly system-associated differentially expressed genes (DEGs) and validated using RT-qPCR, western blotting, and IHC.

**Results:** Implantation of the novel growth-friendly system increased body weight, body length, and total lung volume, as well as decreased the coronal and sagittal Cobb angles for the EOS + TIS model. It also ameliorated EOS + TIS-induced thickening of the alveolar wall, increased alveolar spaces, and decreased alveolar number and diameter. In lung tissue, a total of 790 novel growth-friendly system-associated DEGs were identified, and they were mainly involved in the regulation of immune, inflammatory, calcium transport, and vascular development. Among these DEGs, BDKRB1, THBS1, DUSP1, IDO1, and SPINK5 were hub genes, and their differential expression was consistent with RNA-seq results in lung tissues.

**Conclusion:** The novel growth-friendly system has mitigated scoliosis and pulmonary hypoplasia in the EOS + TIS model. We further elucidate the molecular mechanisms underlying the amelioration of pulmonary hypoplasia.

## 1. Introduction

Early-onset scoliosis (EOS) is distinguished by its precocious emergence and swift exacerbation of spinal curvature. Absent prompt

<sup>\*</sup> Corresponding author. No.374, Dianmian Avenue, Kunming, Yunnan, 650101, China.

E-mail address: [xiejingming@vip.163.com](mailto:xiejingming@vip.163.com) (J. Xie).

<https://doi.org/10.1016/j.heliyon.2024.e27887>

Received 11 September 2023; Received in revised form 6 March 2024; Accepted 7 March 2024

Available online 13 March 2024

2405-8440/© 2024 The Authors. Published by Elsevier Ltd. This is an open access article under the CC BY-NC-ND license (<http://creativecommons.org/licenses/by-nc-nd/4.0/>).

intervention, EOS can gravely impair the development and functionality of the thoracic cage-lung complex in children [1,2]. Thoracic Insufficiency Syndrome (TIS) is a congenital anomaly of the thorax that culminates in compromised respiratory and pulmonary functionality [3]. EOS frequently co-occurs with TIS, establishing a potent interconnection that perpetuates a detrimental cycle. On the one hand, scoliosis causes thoracic deformity, thereby affecting the development and function of the lungs, and is one of the triggers of TIS [4,5]. On the other hand, TIS leads to an imbalance in the muscle groups, which has an impact on the normal growth and development of the spine, leading to EOS [4,5]. Notably, pulmonary hypoplasia, a primary characteristic of patients with the EOS + TIS, induces respiratory failure, which is the main cause of dying prematurely in patients [5,6]. Consequently, there is a pressing necessity to devise secure and effective interventions to ameliorate scoliosis and pulmonary hypoplasia in children with the EOS + TIS.

Currently, posterior procedure employing growth-friendly techniques is the mainstay for children with large and rapidly progressing deformities. It can correct spinal deformities while preserving the growth potential of the spine and supporting heart and lung development [2,7,8]. Growth-friendly techniques mainly consist of distraction-based (traditional growth rods, magnetic controlled growth rods), compression-based (vertebral body stapling), and growth-guided (Luque rods, Shilla rods) techniques [2,7,8]. However, these procedures are not perfect in addressing EOS + TIS and there is currently no recognized treatment approach. Traditional growth rods necessitate multiple distractions, resulting in extremely long treatment cycles and complications [9]. Luque rods and Shilla rods are the main devices in the growth-guided technique. While they allow and guide spinal growth, moderating scoliosis in the process, implantation of pedicle screws in children presents challenging, with the risk of spinal cord injury during treatment [10,11]. Our group has developed a novel growth-friendly system, which is based on a bilateral growth-guided technique. It manages scoliosis without hindering spinal growth, allowing the vertebrae to maintain a degree of rotational flexibility. Multiple surgeries were avoided with this system. Furthermore, it fully accommodates the option of larger diameter rods while being able to minimize the notch of screw tops. However, its therapeutic effect on scoliosis and pulmonary hypoplasia in the EOS + TIS has yet to be evaluated.

It is significant to note that we have previously developed a porcine model of the EOS + TIS [12]. Therefore, the present study intends to comprehensively assess the effects of our system on scoliosis and pulmonary hypoplasia, examining radiological, pathological, and transcriptomic outcomes in this model, while also investigating the underlying molecular mechanisms. It aims to provide

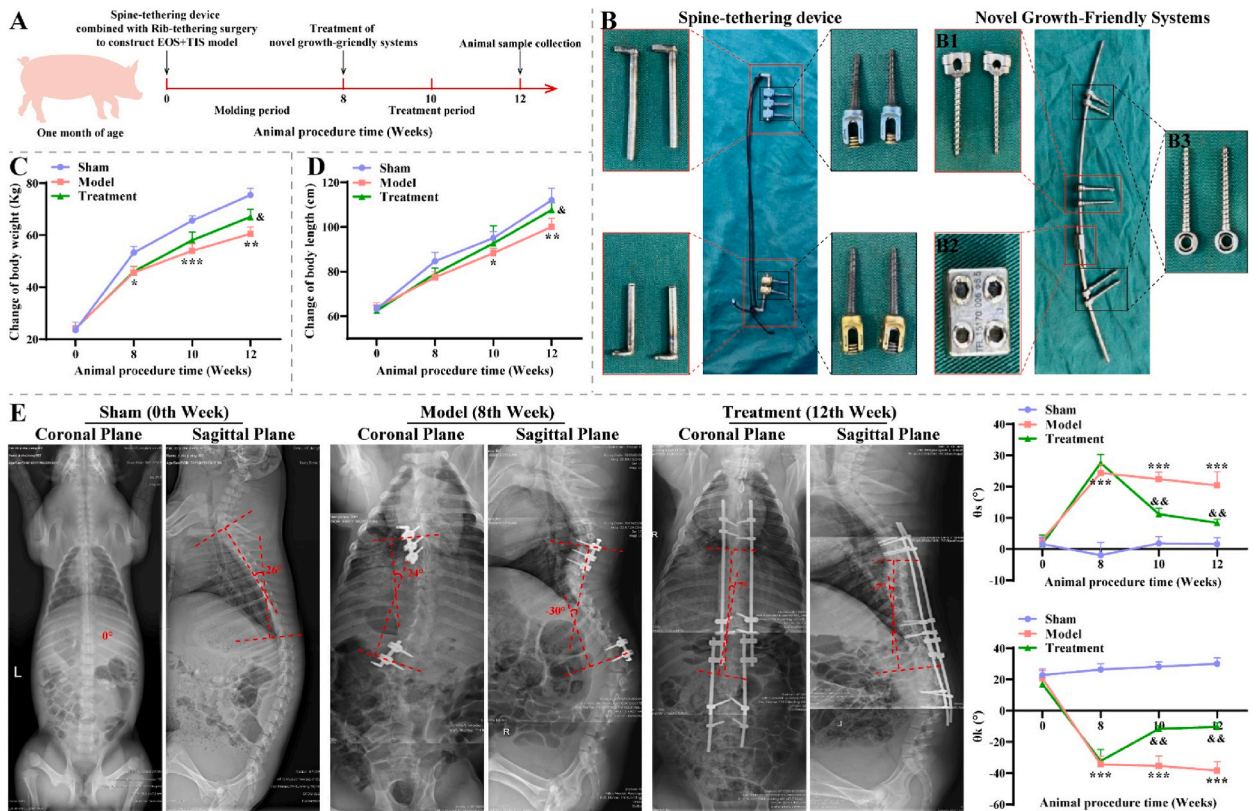


**Fig. 1.** Effect of novel growth-friendly system on scoliosis in the EOS + TIS. A: Flowchart of the animal procedures in this study. B: Overall image of the spine-tethering device and the novel growth-friendly system. B1: Gland screw; B2: Transversal connector; B3: Eye screw. Statistical analysis of piglet weights at 0th, 8th, 10th, and 12th weeks for Sham, Model, and Treatment groups (N = 5). D: Statistical analysis of changes in body length of piglets (N = 5). E: Representative X-ray images of coronal and sagittal planes and statistical analysis of changes in coronal Cobb angle (θs) and sagittal Cobb angle (θk) of piglets at the 0th, 8th, and 12th weeks, respectively (N = 5). Markers are θs and θk for each group of piglets. Compared to the Sham group, \*P < 0.05; \*\*P < 0.01; \*\*\*P < 0.001. Compared to the Model group, &P < 0.05; &&P < 0.01.

more references and perspectives for future EOS + TIS treatments.

## 2. Materials and methods

### 2.1. Wet laboratory research

#### 2.1.1. Animals and ethics

The study was approved by the Ethics Committee of Kunming Medical University (KMMU2020135), and the ARRIVE guidelines were strictly followed. The subjects in this study were genetically unrelated female Yorkshire pigs (1 month old,  $23.9 \pm 2.0$  kg,  $63.1 \pm 1.6$  cm), a total of 15 individuals. All piglets have free access to food and water and are maintained in uniform conditions. Preoperatively, normal alignment of the spine was confirmed in both the sagittal and coronal planes using X-rays. All piglets were adaptively fed for one week and then underwent a surgical procedure.

#### 2.1.2. Surgical procedure

In this study, the animal procedure included Sham, Model, and Treatment groups with 5 Yorkshire pigs in each group. The animal procedure spanned 12 weeks, during which the EOS + TIS model was established over the initial 0–8 weeks, followed by the implantation of the novel growth-friendly system during weeks 8–12 (Fig. 1A). As we previously described [12], the Model and Treatment groups performed the construction of the EOS + TIS model. At 8 weeks, posterior spinal-tethering and rib-tethering devices were removed from piglets in the Model and Treatment groups, and implantation of the novel growth-friendly system was performed in the Treatment group. The Novel growth-friendly system comprises eye screw, gland screw, transversal connector, and orthopaedic rod (Fig. 1B). Briefly, piglets in the Treatment group were bilaterally implanted with eye screws at T4, T5, L2, and L3, and bilaterally implanted with gland screws at T11 and T12. Subsequently, the orthopaedic rod within the eye bolt and gland bolt was interconnected via a transversal connector. Proper correction maneuvers were applied to the spinal curvature to restore the trunk balance. The same operation was performed on the contralateral side. Piglets in the Sham group were exposed only to the vertebrae and ribs and were not treated with posterior spinal-tethering and rib-tethering devices, or the novel growth-friendly system. Other operations were consistent with the Model and Treatment groups. As we previously described [12], X-ray and computed tomography (CT) were performed at the 0th, 8th, 10th, and 12th weeks to assess the spine, thorax, and lungs, coronal ( $\theta_s$ ) and sagittal Cobb angle ( $\theta_k$ ), and total lung volume (TLV). Finally, all piglets were humanely euthanized via electric shock, after which lung tissue was removed for subsequent pathological and transcriptomic analysis.

#### 2.1.3. Pathological analysis

Histopathological changes in piglet lungs were performed by HE staining as we previously described [12]. Moreover, IHC staining was applied to assess the mean optical density values of M1-type macrophage markers (CD68 and iNOS), M2-type macrophage markers (CD206), angiogenesis-associated proteins (VEGFA and VEGFR2), and differentially expressed genes (DEGs). Briefly, lung tissue sections were subjected to antigenic repair using citrate buffer for 10 min. After 1 h blockade with 1% goat serum, the sections were added with primary and secondary antibodies to the target proteins, respectively. Antibody information for the target protein is provided in Supplementary Table 1. Lung tissue sections were stained with hematoxylin stain (Solarbio, CN) for 5 min after color development with a DAB substrate kit (Thermo Fisher, Waltham, MA, USA). After sealing, the sections were subjected to image collection using a BX53 (LED) fluorescence microscope (Olympus, Tokyo, Japan), and the mean optical density values of the target proteins were determined by Image J software (V.1.0; NIH, Bethesda, MD, USA).

#### 2.1.4. RT-qPCR assay

As we previously described [12], RT-qPCR was utilized to detect the expression differences of the hub gene in Sham, Model, and Treatment groups. Primer sequences for the target genes are shown in Supplementary Table 2. GAPDH was used as an internal reference and normalized by the  $2^{-\Delta\Delta Ct}$  method [13].

#### 2.1.5. Western blotting

Expression of BDKRB1, THBS1, calcium pathway-related proteins (CaMKII $\alpha/\delta$ ), and TGF- $\beta$  pathway-related proteins (TGF- $\beta$  and p-Smad3) was detected by western blotting in lung tissues of Sham, Model and Treatment groups. Briefly, total proteins were extracted from lung tissues using RIPA lysate (strong) (Beyotime, CN), and the concentration of total proteins was determined by a NanoDrop spectrophotometer (Thermo Fisher). An equal amount of total protein sample was taken to perform SDS-PAGE electrophoresis, followed by transfer onto a PVDF membrane. After 1 h block with 1% skimmed milk powder (Beyotime), PVDF membranes were incubated with primary and secondary antibodies for the target proteins, respectively. Details on the antibodies are available in Supplementary Table 1. Subsequently, PVDF membranes were color developed using BeyoECL Plus Kit (Beyotime), and images were collected by ChemiDoc MP chemiluminescent gel imaging system (Bio-Rad, Hercules, CA, USA). Grayscale values in gel blot were analyzed using Image J software (V.1.0; NIH, Bethesda, MD, USA).

### 2.2. Dry laboratory research (transcriptomic analysis and bioinformatics)

RNA-seq of lung tissues from Model and Treatment groups was done by Shanghai oebiotech Co. Quality control and bioinformatics analysis of mRNA expression profiles were performed as previously described [12]. A cumulative 68.61G of clean data was generated

from all samples, with individual samples yielding between 6.43G and 7.3G of clean data. The average filtered reads were 91.07% with a distribution of 80.80–95.64%. The average Q30 bases were 91.45 % with a distribution of 91.31–91.58 %. The average GC content was 51.57% with a distribution of 51.31–51.77%.

2.3. Statistical analysis

Western blotting assay was replicated 3 times per group and the rest of the experiments were equipped with 5 replicates. Statistical analysis of all data was performed by GraphPad Prism (V.9.0.0; GraphPad, CA, USA). Student’s t-test or Mann-Whitney *U* test was performed to compare the differences in variables between the two groups. One/two-way ANOVA with Tukey’s multiple comparisons test or Kruskal-Wallis H test with Dunn’s multiple comparisons test was applied to compare differences in variables between multiple groups. *P* < 0.05 indicates statistical significance.

3. Results

As depicted in Fig. 1A, the subjects were 1-month-old piglets, and the animal procedure period was 12 weeks. The construction period of the EOS + TIS model was from 0 to 8 weeks, and the treatment period of the novel growth-friendly system was from 8 to 12 weeks. The structure of the spine-tethering device and the novel growth-friendly system is exhibited in Fig. 1B. During the animal procedure (0–12 weeks), piglets were performed to analyze body weight, body length, and radiology. After the animal procedure (12 weeks), the piglet lungs were implemented for pathology and transcriptomics analysis. All piglets completed the animal procedure without mortality.

3.1. Novel growth-friendly system mitigates scoliosis in the EOS + TIS model

As shown in Fig. 1C, compared to the Sham group, there was a significant reduction in weight from the 8th week onwards in the EOS + TIS model, while the novel growth-friendly system significantly mitigated the weight loss in the 12th week (*P* < 0.05). Similarly, piglets within the EOS + TIS model exhibited a significant decrease in body length in the 10th week, which was reversed by the novel growth-friendly system in the 12th week (Fig. 1D, *P* < 0.05). This suggests that the novel growth-friendly system can enhance the basic

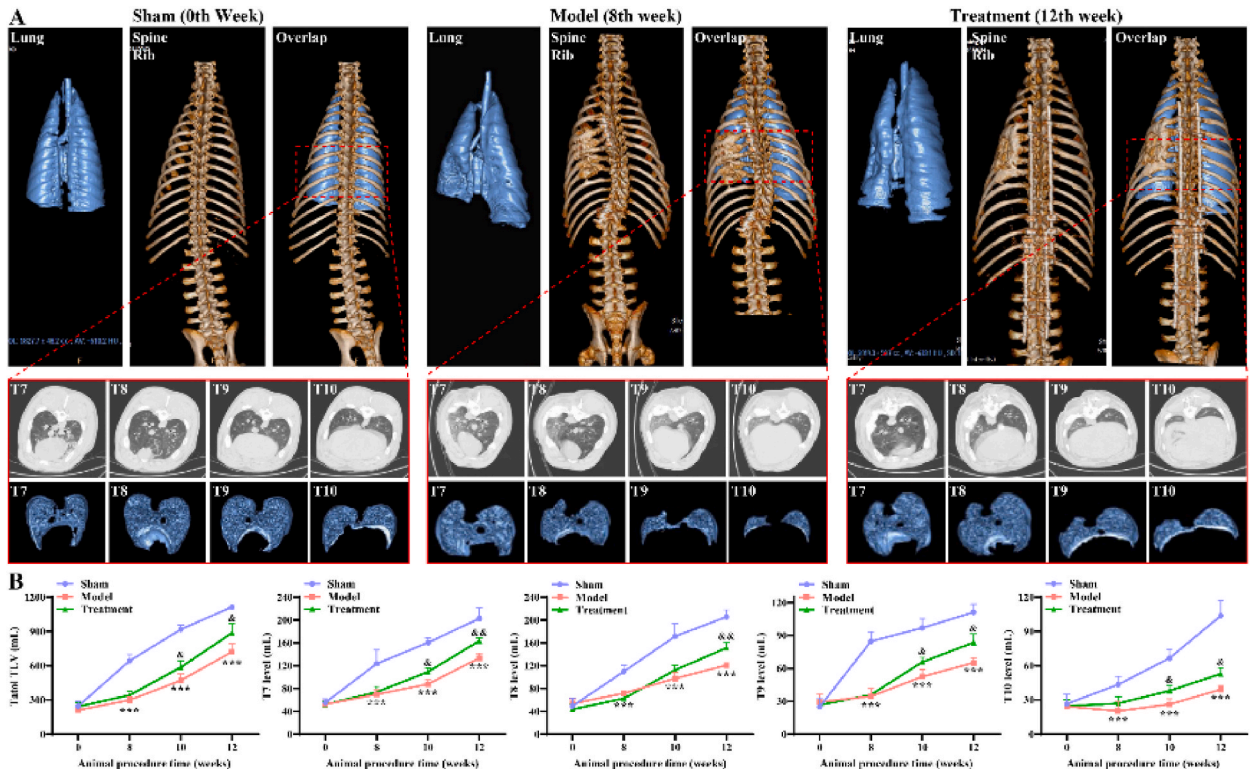


Fig. 2. Effect of novel growth-friendly system on total lung volume in the EOS + TIS. A: (Upper) Representative images of 3D CT reconstruction of the lungs and spine in the Sham, Model, and Treatment groups; (Bottom) Representative pictures of 3D CT reconstruction of the thorax and lungs at the T7-T10 level. B: Statistical analysis of total TLVs and TLVs at the T7-T10 level in all groups of piglets (*N* = 5). Compared to the Sham group, \**P* < 0.05; \*\**P* < 0.01; \*\*\**P* < 0.001. Compared to the Model group, &#x26;#x26;*P* < 0.05; &#x26;#x26;*P* < 0.01.

physique of the EOS + TIS model. Further, we evaluated the effect of the novel growth-friendly system on scoliosis characterization in the EOS + TIS model. As indicated in Fig. 1E, compared to the Sham group,  $\theta_s$  and  $\theta_k$  in the Model group underwent significant alterations from 0 to 8 weeks, with both showing statistical significance at the 8th week ( $P < 0.001$ ). The implantation of the novel growth-friendly system gradually alleviated the changes in  $\theta_s$  and  $\theta_k$  from the 8th week onwards (Fig. 1E,  $P < 0.01$ ). This suggests that the novel growth-friendly system attenuates scoliosis in the EOS + TIS model.

3.2. Novel growth-friendly system alleviates EOS + TIS-induced pulmonary hypoplasia

We further evaluated the changes in lung development through both radiology and pathology. The visible spinal deformity in the Model group corresponded to the previous X-ray (Fig. 2A). In addition, the Model and Treatment groups exhibited obvious rib fusion, asymmetric thorax, and lung deformity, especially in the Model group (Fig. 2A). Since the deformity was mainly manifested at the T7–T10, we further reconstructed 3D images of the thorax and lungs at these levels. The Model and Treatment groups displayed a macroscopic reduction in lung size at the T7–T10 level, especially in the Model group (Fig. 2A). Further, we quantified TLV. The findings indicated a significant reduction in both total TLV and TLV at the T7–T10 level in the Model group compared to the Sham group, beginning from the eighth week onwards (Fig. 2B,  $P < 0.001$ ). After the implantation of the novel growth-friendly system, TLV was significantly improved in the EOS + TIS models (Fig. 2B,  $P < 0.05$ ). This suggests that the implantation of the novel growth-friendly system not only alleviates scoliosis but also provides adequate growth conditions for the lung.

Additionally, we analyzed the effects of the novel growth-friendly system on lung development from a pathological perspective. In the Model group, the alveolar walls appeared markedly thickened and poorly perfused, alongside a reduction in the number of alveoli

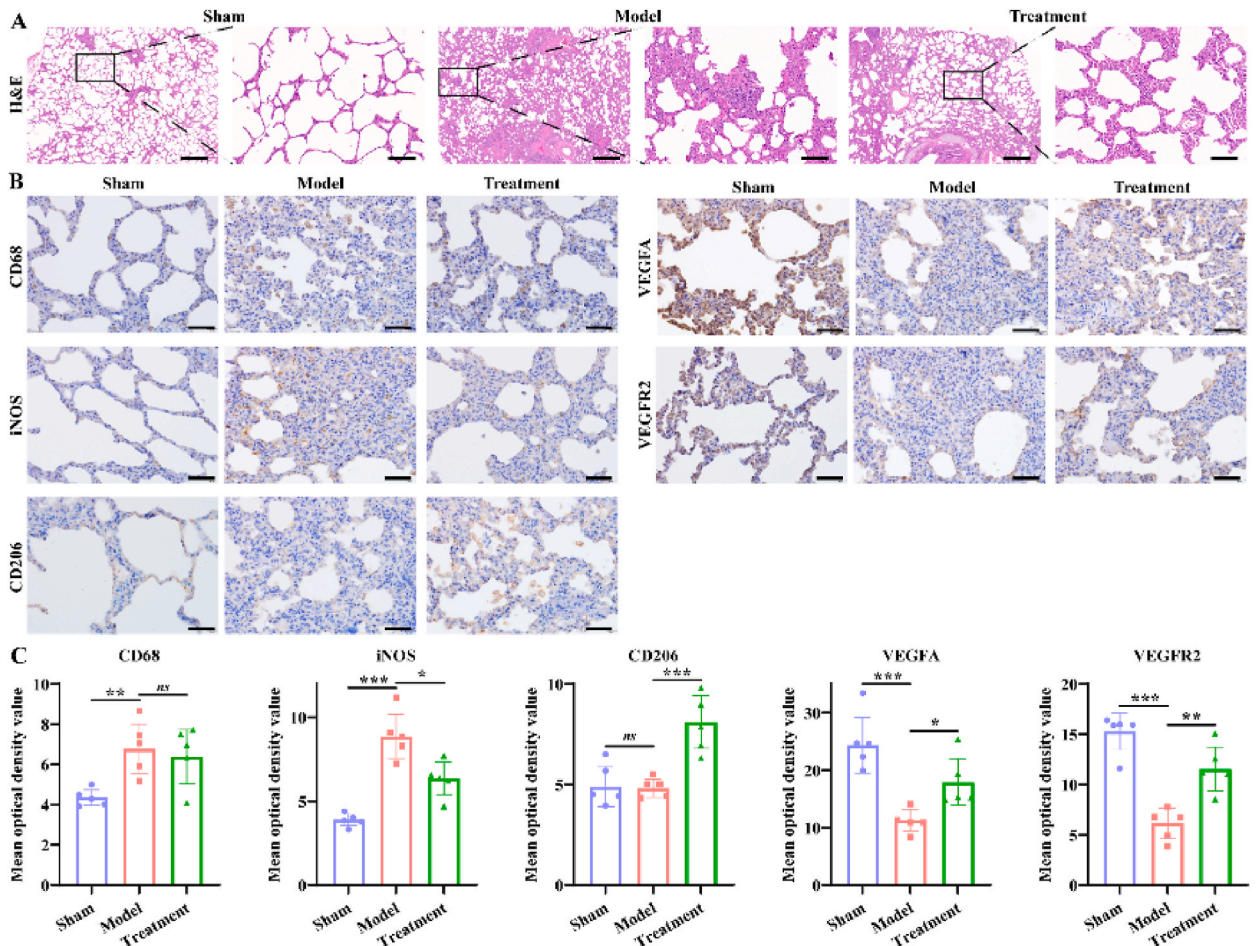
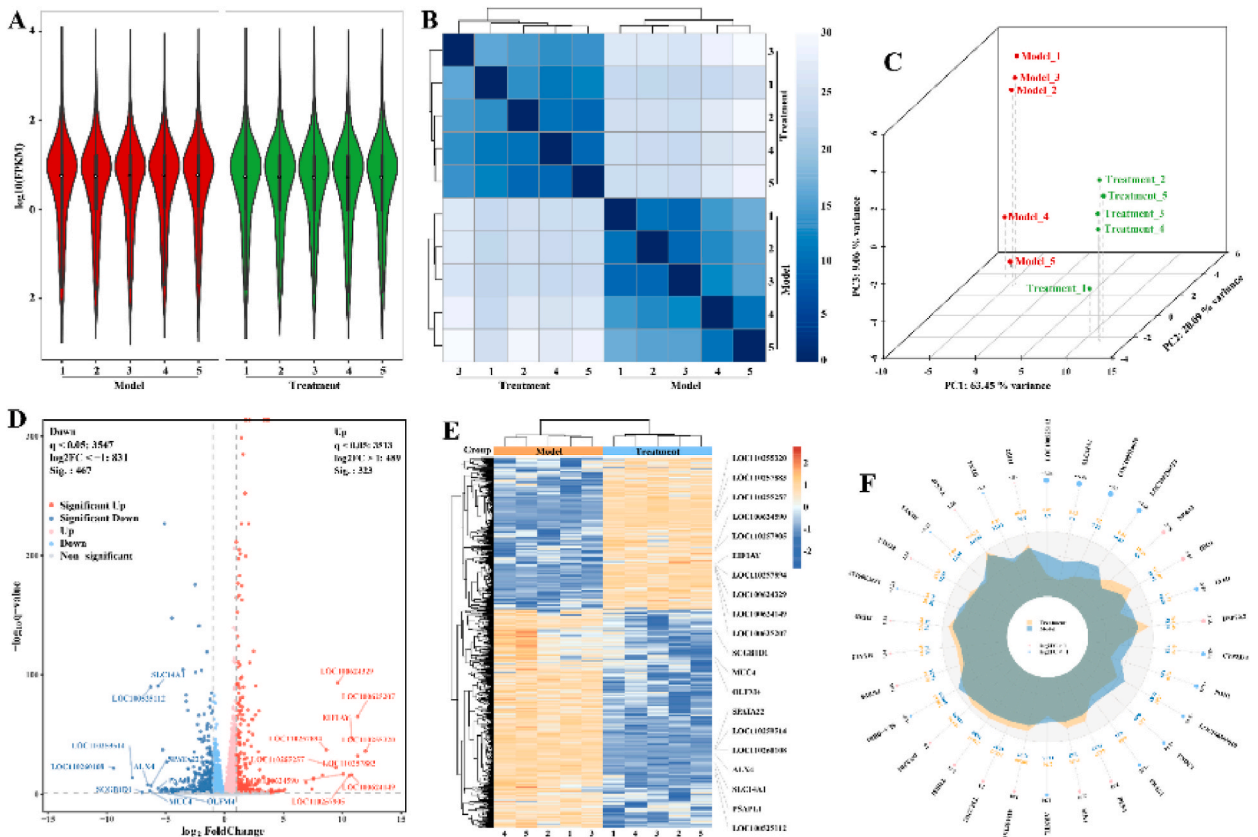


Fig. 3. Effect of novel growth-friendly system on lung histopathology in the EOS + TIS. A: HE staining was applied to observe the pathological changes of lung tissues in the Sham, Model, and Treatment groups. Scale bar: 500  $\mu\text{m}$ . B: IHC staining was performed to detect the effect of the novel growth-friendly system on the expression of M1-type macrophage markers (CD68 and iNOS), M2-type macrophage markers (CD206), and angiogenesis-related proteins (VEGFA and VEGFR2) in lung tissues of the EOS + TIS model. Scale bar: 50  $\mu\text{m}$ . C: Statistical analysis of changes in mean optical density values of CD68, iNOS, CD206, VEGFA, and VEGFR2 for lung tissues in each group ( $N = 5$ ). Compared to the Sham group,  $^*P < 0.05$ ;  $^{**}P < 0.01$ ;  $^{***}P < 0.001$ . Compared to the Model group,  $^{\&}P < 0.05$ ;  $^{\&\&}P < 0.01$ .

and an increase in the alveolar spaces, accompanied by an inflammatory infiltration (Fig. 3A). Notably, these phenomena subsided after treatment (Fig. 3A). Macrophages as the most studied immune cells in lung development. Therefore, we delved deeper into the effect of the novel growth-friendly system on macrophage polarization within the lung. In the Model group, there was a significant increase in CD68 and iNOS, whereas there was no significant change in CD206 (Fig. 3B-C,  $P < 0.01$ ). Significantly, the implantation of a novel growth-friendly system decreased iNOS expression and increased CD206 expression (Fig. 3B-C,  $P < 0.05$ ). Vessels are an important medium for lung development, supplying oxygen and nutrients, promoting alveolar formation, and maintaining normal lung structure. We found that the expression of VEGFA and VEGFR2 was significantly reduced in the Model group, which was alleviated by the implantation of the novel growth-friendly system (Fig. 3B-C,  $P < 0.05$ ). It indicates that a novel growth-friendly system alleviated EOS + TIS-induced pulmonary hypoplasia, which may be achieved by regulating macrophage polarization and angiogenesis.

### 3.3. Identification of novel growth-friendly system-associated DEGs

To understand the molecular mechanism of the novel growth-friendly system for the treatment of EOS + TIS-induced pulmonary hypoplasia at a microscopic level, we performed RNA-seq on lung tissues. Violin plots revealed that the median FPKM of each sample, after normalization, are basically on a level, indicating effective inter-sample normalization (Fig. 4A). Moreover, cluster analysis demonstrated that samples within groups were closer together, while samples between groups were farther apart (Fig. 4B). Similar results were obtained by PCA analysis (Fig. 4C). These results indicate that there is less differentiation in the expression profiles of samples within groups and more differentiation between groups. Differential expression analysis revealed that a total of 790 DEGs were present in the lung tissues of the Treatment group compared to the Model group, which contained 467 significantly down-regulated and 323 significantly up-regulated DEGs (Fig. 4D). The heatmap displayed excellent separation of expression profiles in the Model and Treatment groups, which further enriched the previous results of clustering analysis and PCA (Fig. 4E). The radar plot



**Fig. 4.** Identification of novel growth-friendly system-associated DEGs. **A:** Violin plots display the FPKM values after the normalization of mRNA expression profiles for each sample in the Model and Treatment groups. **B:** Cluster analysis characterizes the distance between the mRNA expression profiles of each sample. Darker colors mean shorter distances. **C:** The mRNA expression profiles of each sample were dimensionalized by principal component analysis (PCA) to characterize the variability. **D:** The volcano plot visualizes the expression of all genes in the Treatment group compared to the Model group. DEGs satisfy both  $|\log_2FC| > 1$  and  $q < 0.05$ . **E:** Heatmap presents the clustering of mRNA expression profiles and the expression of DEGs for each sample. **F:** Radar graph visualizes the FC of DEGs with  $|\log_2FC|$  TOP30. (For interpretation of the references to color in this figure legend, the reader is referred to the Web version of this article.)

showed that LOC100525112, SLC14A1, and LOC100524679 were the lowest expressing DEGs, and NR4A3, IDO1, and HSP70.2 were the highest expressing DEGs (Fig. 4F). It is suggested that these altered expression of DEGs may be one of the reasons for novel growth-friendly system to treat pulmonary hypoplasia.

3.4. GO/KEGG enrichment analysis of novel growth-friendly system-associated DEGs

To understand these DEGs in-depth, we performed GO/KEGG analysis to identify their functions and regulatory pathways. As shown in Fig. 5A, the GO terms enriched by DEGs mainly include "proteinaceous extracellular matrix", "inflammatory response", "immune response", "gluconeogenesis", "calcium ion response", and "blood vessel development". Chord plot showed the DEGs involved in the GO term of the significance TOP 10 (Fig. 5B). Moreover, KEGG enrichment analysis revealed that these DEGs were involved in the "PI3K-Akt signaling pathway", "Cell cycle", "Glycolysis/Gluconeogenesis", "Chemokine signaling pathway", "Calcium signaling pathway", and "TGF-beta signaling pathway" (Fig. 5C-D). This indicates that these DEGs are predominantly extracellular matrix and are mainly involved in the regulation of processes and related pathways that are related to immunity, inflammation, glucose metabolism, calcium transport, and vascular development.

3.5. PPI networks for novel growth-friendly system-associated DEGs

Notably, we have previously characterized DEGs between the Model and Sham groups [12]. Therefore, we intersected the DEGs of

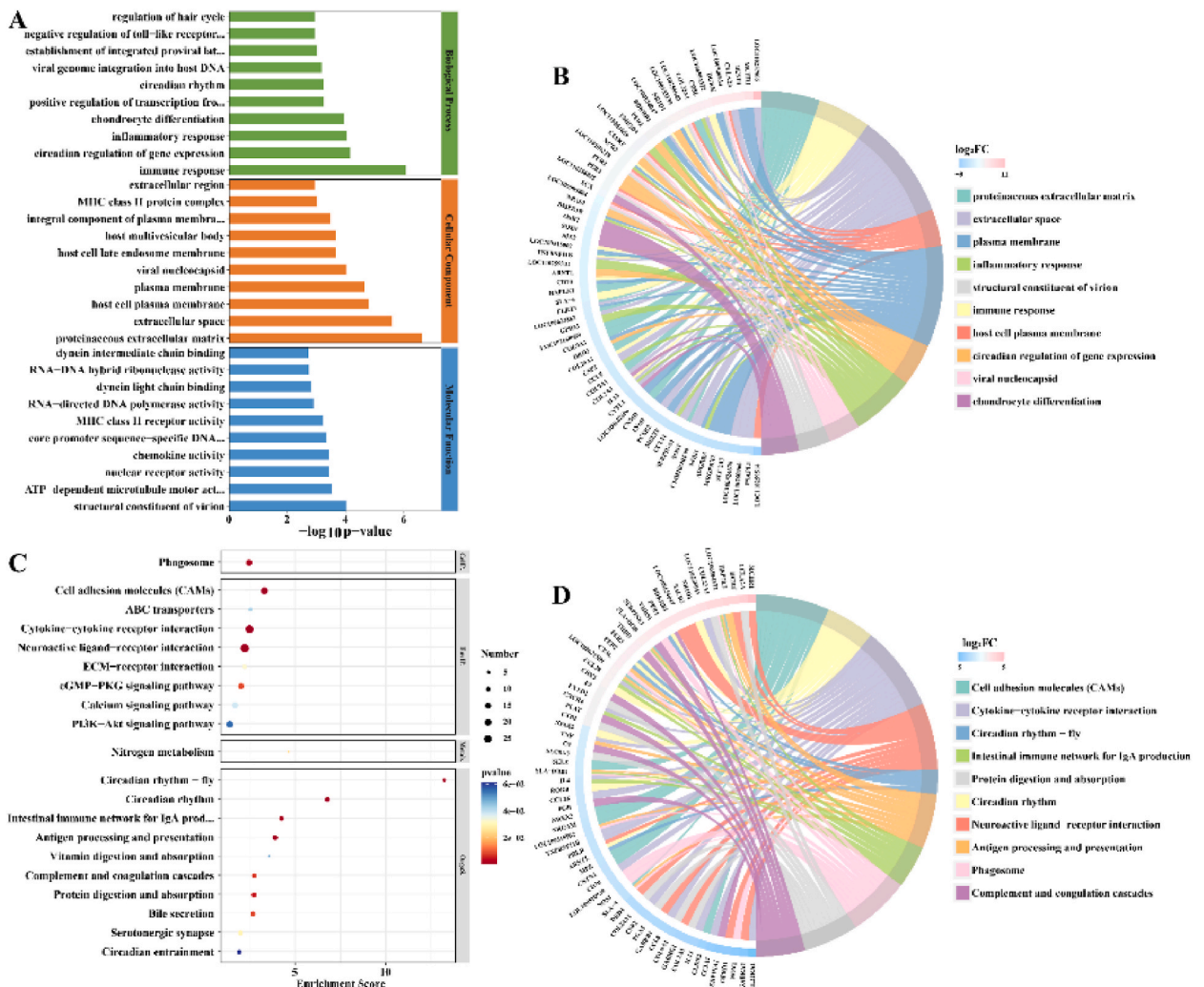


Fig. 5. GO/KEGG enrichment analysis of novel growth-friendly system-associated DEGs. A: Bar plot visualizes the GO terms of the  $-\log_{10}p\text{-value}$  TOP30 obtained by enrichment of the novel growth-friendly system-associated DEGs. B: The chord diagram exhibits the DEGs involved in the GO term for the  $-\log_{10}p\text{-value}$  TOP10. C: Bubble plot visualizes KEGG terms with enrichment score TOP20 obtained by enrichment of the novel growth-friendly system-associated DEGs. D: Enrichment of DEGs in KEGG terms with enrichment score TOP10.

both and obtained 166 overlapping genes (Fig. 6A). To identify key genes in these DEGs, we performed the construction of a PPI network. As shown in Fig. 6B, the network contains 116 nodes and 434 edges. In this network, the genes ranking in the top 5 by degree are RHOB, MX1, RGS, RND1, and THBS1, while those with the top 5 clustering coefficients include CCDC172, SCN4A, MAP1LC3C, ENSSSCP0000022855 and AREG (Fig. 6C). To obtain the key sub-networks in the PPI network, we performed clustering by the MCODE algorithm. The PPI network has a total of seven modular networks (Fig. 6D). The modular network, comprising genes like MX1, KCND3, and SCGN, achieved the highest clustering score (Fig. 6D). It is suggested that these hub genes may play a key role in the novel growth-friendly system for the treatment of EOS + TIS-induced pulmonary hypoplasia.

3.6. Validation of novel growth-friendly system-related DEGs

To characterize the accuracy of RNA-seq, we verified the differential expression of some hub genes in lung tissues using RT-qPCR. In the Model group, the expression of DUSP1, IDO1, SPINK5, C17H8orf4, RGS1, CD5L, THBS1, MYL4, TACR3, BDKRB1, and CHRM1 was significantly decreased compared to Sham group, whereas NRXN2 and SCGN exhibited the opposite trend (Fig. 7A,  $P < 0.01$ ). Moreover, treatment with a novel growth-friendly system restored their expression (Fig. 7A,  $P < 0.05$ ). The results are broadly consistent with RNA-seq (Supplementary Table 3). We selected BDKRB1 and THBS1 for further validation. Western blotting and IHC results demonstrated that the expression differences of BDKRB1 and THBS1 in Sham, Model, and Treatment groups were consistent with RT-qPCR results (Fig. 7B-C,  $P < 0.05$ ). Furthermore, previous KEGG enrichment results revealed that BDKRB1 and THBS1 play roles in modulating the calcium pathway and the TGF- $\beta$  pathway, respectively (Fig. 7D). We found that the expression of proteins associated with the calcium pathway (CaMKII $\alpha/\delta$ ) and the TGF- $\beta$  pathway (TGF- $\beta$  and p-Smad3) was significantly reduced in the Model group, which was reversed by treatment with the novel growth-friendly system (Fig. 7E-F,  $P < 0.05$ ). The above results suggest that BDKRB1- and THBS1-mediated calcium pathways and the TGF- $\beta$  pathway may be potential molecular mechanisms for the novel growth-friendly system therapy.

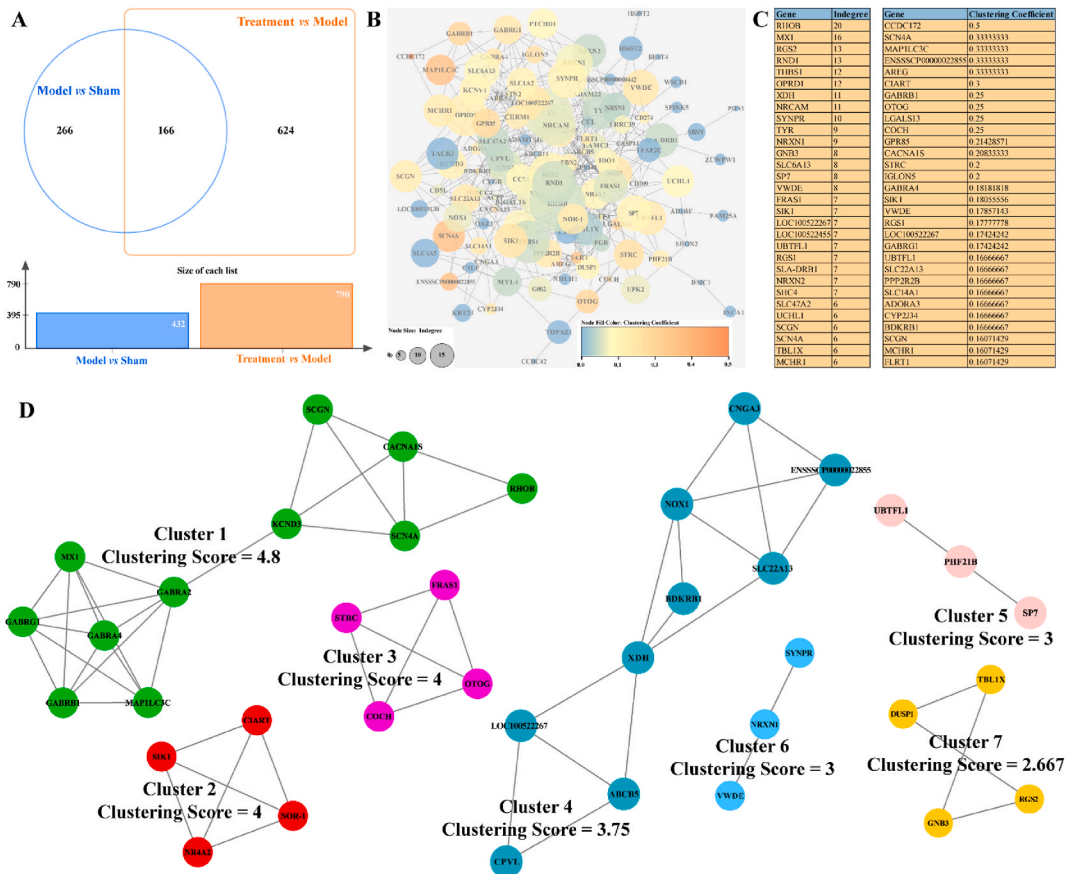
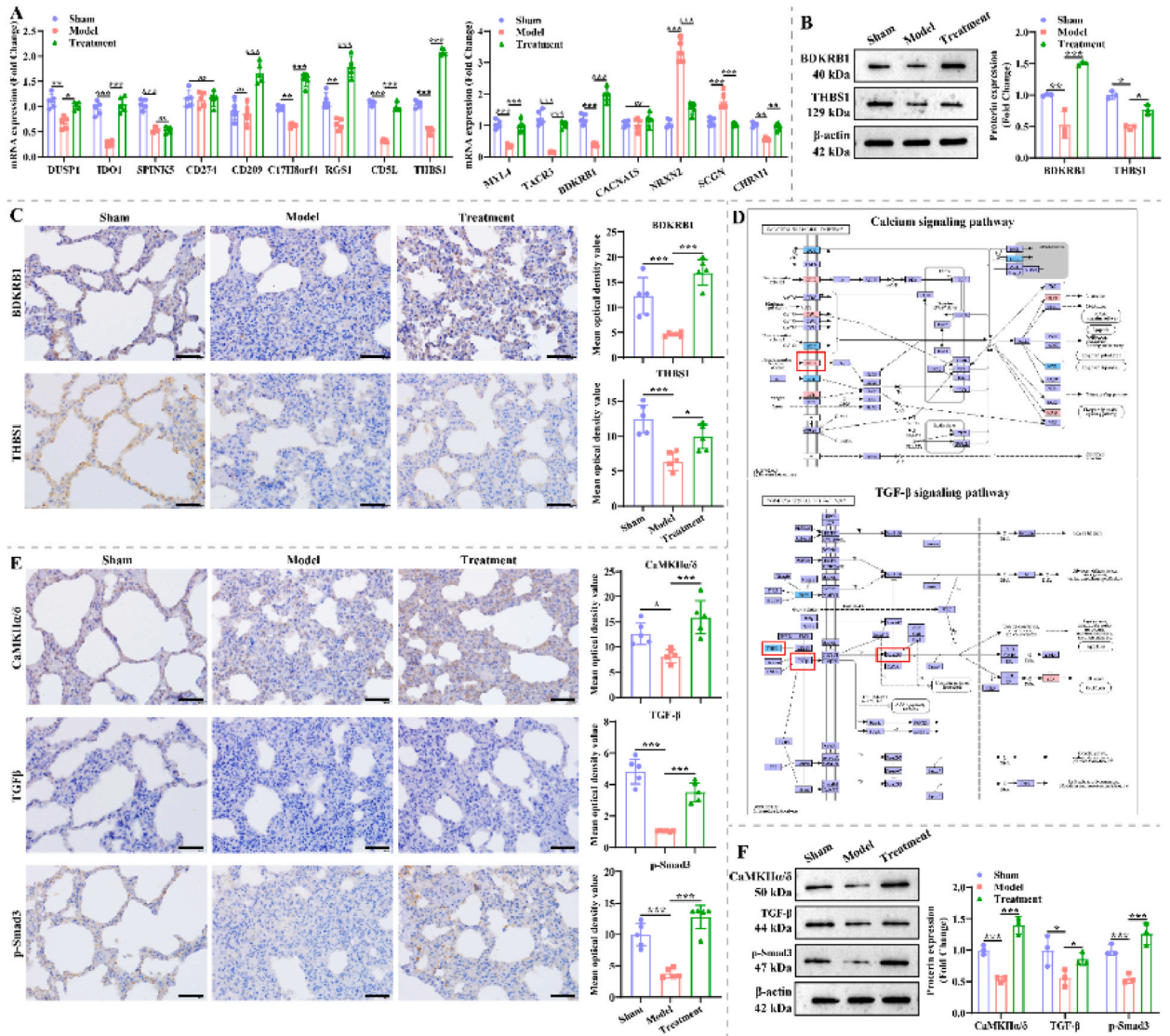


Fig. 6. PPI networks for Novel growth-friendly system-related DEGs. A: Venn diagram visualizes the intersection of DEGs in Model vs Sham and Treatment vs Model. B: A PPI network of the novel growth-friendly system-related DEGs constructed based on the String website, Cytoscape software, and Network Analysis Tool. A larger circle means a larger Indegree and a redder color means a larger clustering coefficient. C: Indegree and clustering coefficient within the TOP30 DEGs in the PPI network of the novel growth-friendly system-related DEGs. D: Cytoscape software and MCODE APP were applied to cluster modules in the PPI network. (For interpretation of the references to color in this figure legend, the reader is referred to the Web version of this article.)



**Fig. 7.** Expression validation of Novel growth-friendly system-associated DEGs. **A:** RT-qPCR was conducted to detect the expression differences of DEGs in lung tissues of Sham, Model, and Treatment groups ( $N = 5$ ). **B:** Representative images of gel blot for BDKRB1 and THBS1 proteins and statistical analysis in lung tissues of each group ( $N = 3$ ). **C:** IHC staining was performed to analyze the mean optical density values of BDKRB1 and THBS1 proteins in lung tissues ( $N = 5$ ). Scale bar: 50  $\mu$ m. **D:** (Upper) Diagram of the calcium pathway involved in BDKRB1; (Bottom) Diagram of the TGF- $\beta$  pathway involved in THBS1. **E:** Representative IHC images of calcium pathway-associated proteins (CaMKII $\alpha/\delta$ ) and TGF- $\beta$  pathway-associated proteins (TGF- $\beta$  and p-Smad3) in lung tissues and their statistical analyses ( $N = 5$ ). Scale bar: 50  $\mu$ m. **F:** Effect of the novel growth-friendly system on the expression of CaMKII $\alpha/\delta$ , TGF- $\beta$ , and p-Smad3 proteins in lung tissues of the EOS + TIS model was detected by western blotting ( $N = 3$ ). The supplementary material provided the original images of gels and blots. \*, \*\*, \*\*\* represent  $P < 0.05$ ,  $P < 0.01$ , and  $P < 0.001$ , respectively; ns represents no significant difference.

#### 4. Discussion

Pulmonary hypoplasia arises from the interplay between EOS and TIS, leading to respiratory failure and, ultimately, patient mortality. As the foremost intervention for the EOS + TIS, posterior procedures utilizing growth-friendly techniques have yielded more favorable outcomes. In the present study, we developed a novel growth-friendly device and evaluated its therapeutic efficacy in a porcine EOS + TIS model. We found that the novel growth-friendly system effectively alleviated scoliosis and pulmonary hypoplasia in the EOS + TIS model. In addition, improvements in lung development may be achieved by altering the mechanical environment of the lung, which modulates processes and relevant pathways such as immunity, inflammation, glucose metabolism, calcium transport, and vascular development.

Novel growth-friendly system belongs to the bilateral growth-guided technique. Presently, the Luque rods and Shilla rods are the

most prevalently utilized devices within the realm of growth-guided techniques. Luque rods were initially recognized for their correction efficacy, with rates varying between 53% and 93%, averaging at 72% [14]. This technique is regarded as highly effective in optimizing the correction of scoliosis deformities [14]. However, subsequent clinical studies have revealed that Luque rods encounter adverse outcomes, including loss of orthopedic angulation, high failure rates of internal fixation, and spontaneous fusion of the spine, forcing the technique to be halted for a time [11,15]. While Ouellet et al. [16] refined the Luque rods to address the shortcomings of their predecessors, the technique still carries the risk of rod grinding and spontaneous fusion of the spine. The Shilla bar was originally developed by McCarthy et al. [17], and they found a correction rate of 67.7% at a 2-year follow-up. A 7-year follow-up indicates a correction rate of 44.3% for the Shilla bar, yet the complication rate stands at 73%, primarily comprising secondary infections and complications related to internal fixation [18]. In the present study,  $\theta_s$  and  $\theta_k$  were corrected from the initial  $(27.6 \pm 2.4)^\circ$  and  $(-32.2 \pm 6.6)^\circ$  to  $(8.4 \pm 1.0)^\circ$  and  $(-10.4 \pm 2.5)^\circ$  with correction rates of 69.57% and 67.70%, respectively, in the porcine EOS + TIS model after a 4-week treatment with the novel growth-friendly system. Compared to the Luque and Shilla rods, the novel growth-friendly system's outcome is excellent from a scoliosis treatment standpoint in only 4 weeks, with no complications or spontaneous fusion of the spine. Moreover, we more comprehensively analyzed the changes in thoracic and lung development. Compared to the EOS + TIS, implantation of the novel growth-friendly system resulted in an increase in TLV from  $(720.3 \pm 61.7)$  ml to  $(816.2 \pm 70.7)$  ml, with a growth rate of 13.3%. Furthermore, treatment with the novel growth-friendly system improved the pathologic features of the lung tissue. These findings suggest that the novel growth-friendly system not only provides excellent correction of scoliosis but also provides an appropriate environment for lung development. At the same time, these findings provide a solid theoretical basis for the clinical application of the novel growth-friendly system, which is more comprehensive than that of the Luque and Shilla rods.

Microarrays, high-throughput sequencing, and bioinformatics-related dry Labs offer more possibilities and developments for the exploration of molecular mechanisms [19–21]. Therefore, we microscopically explored the molecular mechanisms of the novel growth-friendly system on lung development using RNA-seq. We found that RHOB, DUSP1, RGS1, AREG, THBS1, TACR3, BDKRB1, CACNA1S, NRXN2, and CHR1 are the novel growth-friendly system-mediated hub genes for lung hypoplasia. Notably, some of these genes have been identified as being involved in the regulation of lung development. NRXN2 has been demonstrated to exacerbate inflammatory responses in lung tissues [22], while DUSP1 has anti-inflammatory effects [23,24]. AREG facilitates airway remodeling [25], and DUSP1 exhibits anti-pulmonary fibrosis [26]. In the present study, we found that the novel growth-friendly system reversed the down-regulation of DUSP1, AREG, and DUSP1 expression and the up-regulation of NRXN2 expression in the EOS + TIS model. It is suggested that the novel growth-friendly system may alleviate the inflammatory response and fibrosis in the lungs by regulating the expression of NRXN2, DUSP1, and AREG. In addition, THBS1-deficient mice exhibited more severe lung permeability and neutrophilic inflammation [27,28]. Similarly, we found that the novel growth-friendly system upregulated the expression of THBS1, and its downstream TGF- $\beta$  pathway was activated in the EOS + TIS model. Notably, the TGF- $\beta$  pathway is a critical pro-angiogenesis-related pathway in the body [29,30], and abnormal pulmonary angiogenesis is associated with pulmonary hypoplasia [31,32]. Combined with our previous finding the downregulation of angiogenesis-related proteins (VEGFA and VEGFR2) in the EOS + TIS model was reversed by the novel growth-friendly system. We hypothesized that the novel growth-friendly system could activate the TGF- $\beta$  pathway to promote lung angiogenesis by regulating THBS1 expression. Moreover, the novel growth-friendly system regulates genes, which may be achieved by altering the mechanical environment in the lungs. Because it has been demonstrated that gene expression in the lungs responds to changes in mechanical forces [33–35].

Admittedly, there are some shortcomings in this study. For instance, we did not evaluate whether the novel growth-friendly system affected the growth and development of normal piglets. Moreover, it is necessary to extend the treatment period of the novel growth-friendly system to observe whether the EOS + TIS model develops adverse effects. Although the spinal and pulmonary structures of piglets are very similar to those of humans, upright walking and gravity also contributed to the development of the EOS + TIS. Therefore, it is essential to evaluate the novel growth-friendly system in bipeds. These issues are necessary for the clinical application of the novel growth-friendly system. Nevertheless, the novel growth-friendly system does have the ability to correct spinal deformities, indicating its clinical application value.

In conclusion, the present study confirms that the novel growth-friendly system can effectively alleviate scoliosis and pulmonary dysplasia in the porcine EOS + TIS model, and reveals the underlying molecular mechanisms using RNA-seq. These findings will provide a solid theoretical foundation for future applications of the novel growth-friendly system. The novel growth-friendly system offers another possibility for the clinical treatment of the EOS + TIS.

### Ethics approval

This study was approved by the Ethics Committee of the Ethics Committee of Kunming Medical University (KMMU2020135).

### Consent for publication

Not applicable.

### Availability of data and materials

All the data obtained and materials analyzed in this research are available with the corresponding author upon reasonable request.

## Funding

1. National Natural Science Foundation of China (grant No.82060414).
2. Special and Joint Program of Yunnan Provincial Science and Technology Department & Kunming Medical University (Grant No. 202101AY070001-150).
3. Project funded by the "Famous Doctor" Special Fund of Yunnan Revitalization Talent Support Program (Zhang Ying in 2022-XDYC-MY-2022-0026).

## CRedit authorship contribution statement

**Ying Zhang:** Writing – original draft, Visualization, Validation, Methodology, Investigation, Funding acquisition, Formal analysis, Conceptualization. **Quan Li:** Writing – original draft, Visualization, Validation, Methodology, Formal analysis. **Zhiyue Shi:** Writing – original draft, Visualization, Validation, Methodology, Formal analysis. **Qitang Li:** Writing – review & editing, Visualization, Validation, Formal analysis, Data curation. **Xinfei Dai:** Writing – review & editing, Visualization, Validation, Resources, Formal analysis. **Cheng Pan:** Writing – review & editing, Visualization, Validation, Formal analysis, Data curation. **Yujian Ma:** Writing – review & editing, Visualization, Validation, Formal analysis. **Rongshuang Yan:** Writing – review & editing, Visualization, Validation, Formal analysis. **Derui Fei:** Writing – review & editing, Visualization, Validation, Formal analysis. **Jingming Xie:** Writing – review & editing, Project administration, Funding acquisition, Conceptualization.

## Declaration of competing interest

The authors declare that they have no known competing financial interests or personal relationships that could have appeared to influence the work reported in this paper.

## Acknowledgements

Not applicable.

## Appendix A. Supplementary data

Supplementary data to this article can be found online at <https://doi.org/10.1016/j.heliyon.2024.e27887>.

## References

- [1] G. Ruiz, N.J. Torres-Lugo, P. Marrero-Ortiz, H. Guzmán, G. Olivella, N. Ramírez, Early-onset scoliosis: a narrative review, *EFORT open reviews* 7 (8) (2022) 599–610.
- [2] Y.B. Zhang, J.G. Zhang, Treatment of early-onset scoliosis: techniques, indications, and complications, *Chin. Med. J.* 133 (3) (2020) 351–357.
- [3] K. Tsukahara, O.H. Mayer, Thoracic insufficiency syndrome: approaches to assessment and management, *Paediatr. Respir. Rev.* 44 (2022) 78–84.
- [4] L.A. Karol, The natural history of early-onset scoliosis, *Journal of pediatric orthopedics* 39 (6) (2019) S38–s43. Supplement 1 Suppl 1.
- [5] Y. Wang, D. Wang, G. Zhang, B. Ma, Y. Ma, Y. Yang, S. Xing, X. Kang, B. Gao, Effects of spinal deformities on lung development in children: a review, *J. Orthop. Surg. Res.* 18 (1) (2023) 246.
- [6] D.D. Sheehan, J. Grayhack, Pulmonary implications of pediatric spinal deformities, *Pediatr. Clin.* 68 (1) (2021) 239–259.
- [7] A. Senkoylu, R.B. Riise, E. Acaroglu, I. Helenius, Diverse approaches to scoliosis in young children, *EFORT open reviews* 5 (10) (2020) 753–762.
- [8] V. Cunin, Early-onset scoliosis: current treatment, *Orthopaedics & traumatology, surgery & research : OTSR* 101 (1 Suppl) (2015) S109–S118.
- [9] S. Bekmez, O. Dede, M. Yazici, Advances in growing rods treatment for early onset scoliosis, *Curr. Opin. Pediatr.* 29 (1) (2017) 87–93.
- [10] D.J. Quint, G. Salton, Migration of luque rods through a laminectomy defect causing spinal cord compression, *AJNR. American journal of neuroradiology* 14 (2) (1993) 395–398.
- [11] L.A. Rinsky, J.G. Gamble, E.E. Bleck, Segmental instrumentation without fusion in children with progressive scoliosis, *Journal of pediatric orthopedics* 5 (6) (1985) 687–690.
- [12] Y. Zhang, Z. Shi, W. Li, X. Dai, Q. Li, C. Pan, R. Yan, Y. Ma, D. Fei, J. Xie, A porcine model of early-onset scoliosis combined with thoracic insufficiency syndrome: construction and transcriptome analysis, *Gene* 858 (2023) 147202.
- [13] K.J. Livak, T.D. Schmittgen, Analysis of relative gene expression data using real-time quantitative PCR and the 2(-Delta Delta C(T)) Method, *Methods (San Diego, Calif.)* 25 (4) (2001) 402–408.
- [14] E.R. Luque, Segmental spinal instrumentation for correction of scoliosis, *Clin. Orthop. Relat. Res.* (163) (1982) 192–198.
- [15] C.F. Eberle, Failure of fixation after segmental spinal instrumentation without arthrodesis in the management of paralytic scoliosis, the *Journal of bone and joint surgery, American volume* 70 (5) (1988) 696–703.
- [16] J. Ouellet, Surgical technique: modern Luqué trolley, a self-growing rod technique, *Clin. Orthop. Relat. Res.* 469 (5) (2011) 1356–1367.
- [17] R.E. McCarthy, S. Luhmann, L. Lenke, F.L. McCullough, The Shilla growth guidance technique for early-onset spinal deformities at 2-year follow-up: a preliminary report, *Journal of pediatric orthopedics* 34 (1) (2014) 1–7.
- [18] R.E. McCarthy, F.L. McCullough, Shilla growth guidance for early-onset scoliosis: results after a minimum of five years of follow-up, the *journal of bone and joint surgery, American volume* 97 (19) (2015) 1578–1584.
- [19] P. Behzadi, R. Ranjbar, DNA microarray technology and bioinformatic web services, *Acta Microbiol. Immunol. Hung.* 66 (1) (2019) 19–30.
- [20] S. Wang, S.T. Sun, X.Y. Zhang, H.R. Ding, Y. Yuan, J.J. He, M.S. Wang, B. Yang, Y.B. Li, The evolution of single-cell RNA sequencing technology and application: progress and perspectives, *Int. J. Mol. Sci.* 24 (3) (2023).
- [21] X. Ling, C. Wang, L. Li, L. Pan, C. Huang, C. Zhang, Y. Huang, Y. Qiu, F. Lin, Y. Huang, Third-generation sequencing for genetic disease, *Clinica chimica acta, international journal of clinical chemistry* 551 (2023) 117624.

- [22] D.E. Kennedy II, P. Mody, J.F. Gout, W. Tan, K.S. Seo, A.K. Olivier, J.W. Rosch, J.A. Thornton, Contribution of puma to inflammatory resolution during early pneumococcal pneumonia, *Front. Cell. Infect. Microbiol.* 12 (2022) 886901.
- [23] J. Li, S. Liu, LncRNA GAS5 suppresses inflammatory responses and apoptosis of alveolar epithelial cells by targeting miR-429/DUSP1, *Exp. Mol. Pathol.* 113 (2020) 104357.
- [24] Y.H. Ding, R.X. Miao, Q. Zhang, Hypaphorine exerts anti-inflammatory effects in sepsis induced acute lung injury via modulating DUSP1/p38/JNK pathway, *Kaohsiung J. Med. Sci.* 37 (10) (2021) 883–893.
- [25] W.H. Cheng, S.Y. Kao, C.L. Chen, F.S. Yuliani, L.Y. Lin, C.H. Lin, B.C. Chen, Amphiregulin induces CCN2 and fibronectin expression by TGF- $\beta$  through EGFR-dependent pathway in lung epithelial cells, *Respir. Res.* 23 (1) (2022) 381.
- [26] L.R.K. Penke, J. Speth, S. Wettlaufer, C. Draijer, M. Peters-Golden, Bortezomib inhibits lung fibrosis and fibroblast activation without proteasome inhibition, *Am. J. Respir. Cell Mol. Biol.* 66 (1) (2022) 23–37.
- [27] H.F. Peñaloza, T.F. Olonisakin, W.G. Bain, Y. Qu, R. van der Geest, J. Zupetic, M. Hulver, Z. Xiong, M.W. Newstead, C. Zou, J.K. Alder, J.A. Ybe, T.J. Standiford, J.S. Lee, Thrombospondin-1 restricts Interleukin-36 $\gamma$ -mediated neutrophilic inflammation during *Pseudomonas aeruginosa* pulmonary infection, *mBio* 12 (2) (2021).
- [28] Y. Qu, T. Olonisakin, W. Bain, J. Zupetic, R. Brown, M. Hulver, Z. Xiong, J. Tejero, R.M. Shanks, J.M. Bomberger, V.S. Cooper, M.E. Zegans, H. Ryu, J. Han, J. Pilewski, A. Ray, Z. Cheng, P. Ray, J.S. Lee, Thrombospondin-1 protects against pathogen-induced lung injury by limiting extracellular matrix proteolysis, *JCI insight* 3 (3) (2018).
- [29] Y. Zhang, X. Yang, The roles of TGF- $\beta$  signaling in Cerebrovascular diseases, *Front. Cell Dev. Biol.* 8 (2020) 567682.
- [30] T. Watabe, K. Takahashi, K. Pietras, Y. Yoshimatsu, Roles of TGF- $\beta$  signals in tumor microenvironment via regulation of the formation and plasticity of vascular system, *Semin. Cancer Biol.* 92 (2023) 130–138.
- [31] C.M. Alvira, Aberrant pulmonary vascular growth and remodeling in Bronchopulmonary dysplasia, *Front. Med.* 3 (2016) 21.
- [32] B. Thébaud, Angiogenesis in lung development, injury and repair: implications for chronic lung disease of prematurity, *Neonatology* 91 (4) (2007) 291–297.
- [33] E.C. Breen, Z. Fu, H. Normand, Calyculin gene expression is increased by mechanical strain in fibroblasts and lung, *Am. J. Respir. Cell Mol. Biol.* 21 (6) (1999) 746–752.
- [34] B.L.M. Hogan, Integrating mechanical force into lung development, *Dev. Cell* 44 (3) (2018) 273–275.
- [35] A. Marchioni, R. Tonelli, S. Cerri, I. Castaniere, D. Andrisani, F. Gozzi, G. Bruzzi, L. Manicardi, A. Moretti, J. Demurtas, S. Baroncini, A. Andreani, G.F. Cappiello, S. Busani, R. Fantini, L. Tabbi, A.V. Samarelli, E. Clini, Pulmonary stretch and lung mechanotransduction: implications for progression in the fibrotic lung, *Int. J. Mol. Sci.* 22 (12) (2021).